LANGMUIR

pubs.acs.org/Langmuir Article

Comparative Degradation Kinetics Study of Polyamide Thin Films in Aqueous Solutions of Chlorine and Peracetic Acid Using Quartz Crystal Microbalance

Tashfia M. Mohona, Ning Dai,* and Prathima C. Nalam*

Cite This: https://doi.org/10.1021/acs.langmuir.1c02835 Read Online

ACCESS | Metrics & More | Article Recommendations | Supporting Information

ABSTRACT: Polyamide thin film composite membranes are widely used in water reclamation. Peracetic acid (PAA) is an emerging wastewater disinfectant with a potential for membrane cleaning and disinfection; however, its interaction with polyamide remains poorly understood. This study employs quartz crystal microbalance with dissipation (QCM-D) to determine the PAA-induced degradation kinetics of polyamide thin films, in comparison with the conventional disinfectant-free chlorine (HOCl). Polyamide films showed a sorption phase followed by a degradation phase when exposed to PAA (1000 mg L^{-1}) and HOCl (100 mg L^{-1}) solutions. While the sorption phase in HOCl experiments was short (1.4−3.5 min) and followed a Boltzmann-sigmoidal model, it spanned over 3−33 h in PAA experiments and displayed a two-stage behavior. The latter kinetics are attributed to sequential processes of the physical sorption of PAA in polyamide films followed by PAA-induced polyamide oxidation. In the degradation phase, the HOCl-exposed films followed a rapid, two-step exponential decay reaching an equilibrium mass of ∼50% of the initial (wet) mass after ∼5 h of exposure. In contrast, the PAA-exposed films followed a Boltzmann-sigmoidal decay, with ∼80% of the initial (wet) mass remaining intact after >10 h of exposure. Fast force maps generated using atomic force microscopy showed a progressive increase in the morphological heterogeneity of the polyamide films in HOCl solution due to pitting, cracking, bulging, and eventual delamination under both flow and no-flow conditions. In contrast, PAA only formed small pits on the polyamide film under flow; in a stagnant PAA solution, the film had no visible changes even after ∼148 h of exposure. This is the first comparative study on the chemical and morphological changes in polyamide films induced by PAA and HOCl. The much higher compatibility of polyamide with PAA than with chlorine supports the potential of PAA being used as a halogen-free membrane cleaning/disinfecting agent.

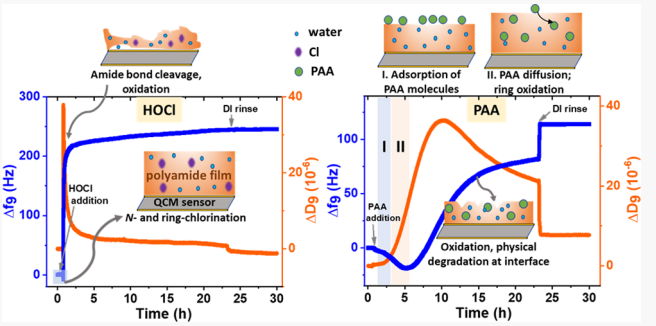

INTRODUCTION

Polyamide thin film composite membranes are widely used in water reclamation and desalination owing to their high selectivity and water permeability.[1−4] In these membrane systems, oxidants such as chlorine species (e.g., chloramine)[5] and peroxides (e.g., hydrogen peroxide)[6] are often used as continuous feed to suppress (bio)fouling or used during periodic cleaning to remove the materials built up on the membrane surface. However, exposure to the oxidants can disrupt the structural integrity of the polyamide active layer, leading to a loss in membrane performance. Among the various oxidants, free chlorine is the most widely investigated,[2,3,7−10] which showed a drastic alteration in membrane performance at exposure concentrations as low as 2−2.5 mg h L^{-1}.[10] Chlorine exposure to polyamide results in *N*-chlorination of the amide bonds and ring chlorination, as well as increased surface oxygen functional groups such as carboxylic acid and quinone.[2,3,7,8,11,12] Hydrogen peroxide (H_2O_2) is another commonly used membrane cleaning agent, which showed higher compatibility with polyamide in comparison to free chlorine. For example, no change in membrane performance was observed up to 17 000 g h L^{-1} exposure of H_2O_2.[13,14] However, in the presence of trace amounts of transition metals such as iron, H_2O_2 can form hydroxyl radicals *via* Fenton reaction and accelerates polyamide degradation.[14,15]

Recently, peracetic acid (PAA), an organic peroxide, is proposed as a promising oxidant for membrane cleaning.[6,16] PAA has approximately 100-fold greater disinfection strength than H_2O_2[17] and exhibits comparable bacterial inactivation as free chlorine in laboratory-based[18] and pilot-scale[19,20] studies. To date, only two studies examined PAA interactions with

Received: October 25, 2021
Revised: November 3, 2021

polyamide using commercial membranes.[16,21] No significant change in membrane performance was observed upon PAA exposure up to 180 g h L^{-1}.[21] In addition, unlike H_2O_2, PAA does not accelerate the deterioration of membrane performance in the presence of iron.[21] However, surface characterization suggested that polyamide could react with PAA to form new oxygen functional groups.[21] More studies are warranted to provide a detailed characterization of the PAA-induced morphological and chemical stability/change of polyamide to provide mechanistic insight into PAA−polyamide interaction.

Quartz crystal microbalance with dissipation (QCM-D) is a surface-sensitive technique well suited to probe interactions between surface and solute molecules *in situ* and real time, providing insights into the mechanisms and kinetics of microscopic processes with environmental and engineering relevance.[22−24] QCM-D is extensively employed to study the physical/chemical sorption of solutes on surfaces[24,25] and to probe the physicochemical changes of soft, solvated surfaces such as polymer films.[26] In particular, viscoelastic properties of thin films originating from solvent-based swelling, conformational changes, and/or degradation processes can be captured.[26−29] For example, QCM-D has been employed extensively to investigate the enzymatic degradation of polymers such as cellulose,[30,31] proteins,[32−34] polyesters,[35−37] and nanogels.[38] QCM-D has also been used to understand polyamide membrane−foulant interaction mechanisms.[39−47] To date, only one study utilized this technique to investigate the oxidant-induced polyamide degradation,[48] which focused on the conventional disinfectant-free chlorine. The study showed that the polyamide film experienced an initial mass gain attributable to chlorine sorption and a subsequent mass loss attributable to film disintegration.[48] A similar technique is expected to provide molecular insight into PAA−polyamide interactions.

In this study, we employed QCM-D to examine the interaction between the novel disinfectant PAA and the polyamide thin films synthesized by a molecular layer-by-layer (mLBL) approach. The results are compared with the experiments conducted with free chlorine. The chlorine experiments provided a useful basis for assessing the PAA−polyamide interaction because the chlorine−polyamide interaction mechanism has been extensively studied using commercial membranes[2,3,7−9,11,49−51] and was also investigated using QCM-D.[48] The sorption and degradation profiles of the polyamide films upon oxidant exposure in QCM-D experiments were fitted to appropriate kinetic models. The type of models and the associated kinetic constants were compared between PAA and chlorine experiments. Additionally, we probed the chemical and morphological changes of the oxidant-exposed polyamide films using X-ray photoelectron spectroscopy (XPS) and atomic force microscopy (AFM). Under both flow and no-flow conditions, PAA induced less oxidative degradation of the polyamide film than free chlorine. The kinetic modeling also suggested that the PAA−polyamide interaction mechanism involves multiple co-occurring physical/chemical processes.

MATERIALS AND METHODS

Materials. 1,3,5-Benzenetricarbonyl trichloride (trimesoyl chloride, TMC, 98%) and *m*-phenylenediamine (MPD, 99%) were purchased from Fisher Scientific, and used as received. Acetone (>99.5%, Alfa Aesar) and toluene (anhydrous 99.8%, Alfa Aesar) were used after molecular sieve drying (Type 3 Å, Sigma-Aldrich). TMC, MPD, and the solvents were stored in a glovebox under a reduced atmosphere (Argon, Mbraun Labmaster 130). Syringes (3 mL, rubber-free, VWR), hypodermic needles (21G × 1 1/2, Fisherbrand), and syringe filters (0.2 μm poly(tetrafluoroethylene), PTFE, Fisherbrand) were used for handling solutions. Silicon wafers with a 50 nm thick oxide layer (University Wafer) and silicon dioxide-coated QCM sensors (QSX 303, NanoScience Instruments) were used as substrates for the deposition of polyamide films. Sodium hypochlorite (5% available chlorine, Ricca Chemical Company) and peracetic acid (32 wt % in dilute acetic acid, 5.4 wt % H_2O_2, Sigma-Aldrich) were stored at 4 °C. Further, a recent study[21] showed that the loss of polyamide membrane performance by PAA is not accelerated in the presence of ferrous iron, at either low or high H_2O_2/PAA ratios. Therefore, in this present study, we did not employ iron-containing solutions to avoid the additional mass (from ions) during QCM measurements. Fresh solutions of these two oxidants were prepared in water before each experiment. All aqueous solutions were prepared in deionized (DI) water (18.1 MΩ·cm). Sodium chloride (NaCl, 99.8%, Fisher Scientific) and acetic acid (glacial, ReagentPlus, ≥99%, Sigma-Aldrich) were used to prepare NaCl and sodium acetate (NaAc) solutions for control experiments, respectively. Sodium hydroxide (NaOH, 99.1%, Fisher Scientific) and hydrochloric acid (HCl, 2.0 N, EMD Millipore) were used for pH adjustment.

Synthesis of Polyamide Films. A spin-coating-assisted molecular layer-by-layer (mLBL) approach was adopted from the literature to deposit the polyamide film on a silica substrate.[47,52−56] The polyamide films prepared by the mLBL method are structurally similar to the active polyamide layer of commercial membranes prepared by the interfacial polymerization method, but the mLBL films have lower roughness.[53] Compared to other methods of preparing polyamide films on QCM,[39,46,57−60] we opted to use the mLBL method because it allows comparison with the only QCM polyamide degradation study (focusing on chlorine)[48] and because the smoother surface can minimize heterogeneity-induced effects on the observed polyamide degradation kinetics. The mLBL procedure involves an alternate deposition of TMC and MPD solutions on the substrate, with a solvent (toluene or acetone) rinse step between each monomer deposition step. Solutions of 1 wt % TMC and MPD were prepared separately in anhydrous toluene. MPD solutions were additionally stirred for ∼1 h until no visible flakes remained. Solutions were filtered through a 0.2 μm PTFE filter. Toluene and acetone were dried overnight with molecular sieves at a 4:1 mass ratio of solvent to dried zeolite prior to use. To minimize the exposure to air and moisture, all solvents and solutions were prepared inside a glovebox and taken out of the controlled environment right before the spin-coating step.

Before polyamide deposition, silica wafers or silica-coated QCM sensors were sonicated in isopropanol and ethanol, sequentially, for 15 min each, to remove organic contamination. The substrates were then sonicated in DI water for 15 min and UV−ozone-cleaned (UV/ozone Procleaner, Nanoscience) for 30 min. The wafers/QCM sensors were not completely dried before placing in the UV−ozone chamber. The UV−ozone treatment step further removes residual organic contaminants and facilitates the formation of a layer of hydroxyl functional groups on the silica surface (using oxygen radicals) to assist TMC−substrate interactions in the subsequent polyamide synthesis steps.[61,62] The cleaned wafers/QCM sensors were then immediately used for polymer deposition.

An aliquot (∼500 μL) of TMC solution was first dropped on the silica wafer/QCM sensor using a syringe and allowed to sit for 15 s to promote covalent bond formation between TMC and the hydroxyl groups on the substrate. The residual solution was removed from the surface by spinning the sample at 3000 rpm for 15 s. Anhydrous toluene (∼500 μL) was then added to the substrate and was held for 15 s before rinsing it off at 4000 rpm to remove unreacted TMC. In the next step, an aliquot (∼500 μL) of MPD solution was added to the TMC-deposited substrate; amide bonds are formed between the free acyl chloride groups on the surface and the amine groups on MPD. Anhydrous acetone (∼500 μL) was then added to the substrate and was held for 15 s before rinsing it off at 4000 rpm to remove

https://doi.org/10.1021/acs.langmuir.1c02835
Langmuir XXXX, XXX, XXX−XXX

unreacted MPD. Acetone instead of toluene was used for the rinse step due to the relatively low solubility of MPD in toluene.[53] These four sequential steps generated one bilayer on the substrate. The process was repeated 15 times to form a thin polyamide film. For QCM sensors, the backside of the sensor was cleaned with an acetone-drenched Q-tip after each cycle to remove any unintentionally accumulated polymer. After polyamide deposition, the substrates were annealed at 215 °C for 1 min on an aluminum-covered hot plate. The samples were stored overnight in a vacuum desiccator for further annealing. The high-temperature annealing step was critical to enhance the bonding between the substrate and the polyamide film.

Quartz Crystal Microbalance with Dissipation (QCM-D) Measurements. The oxidant sorption and oxidative degradation kinetics of the polyamide films were analyzed using QCM-D (E4 model, Q-Sense Inc., Biolin Scientific). Before each measurement, QCM parts such as tubing, O-rings, and flow modules were rinsed thoroughly with isopropanol and ethanol and dried in nitrogen gas (UHP-300, Airgas). All solutions used for QCM measurements were degassed (sonicated) for at least ∼30 min to prevent measurement artifacts caused by air bubbles.

All QCM experiments were conducted at 25 °C and with a flow rate of 50 μL min^{-1}. Oxidant solutions (100 mg L^{-1} of free chlorine or 1000 mg L^{-1} of PAA) were adjusted to pH 6.5 by 1 N HCl (for chlorine) or 1 N NaOH (for PAA). In our experiments, we specially chose pH 6.5 for the following reasons: (1) pH 6.5 lies within the range of typical wastewater pH, i.e., between 6 and 8. Within this range, the polyamide surface remains negatively charged (isoelectric point of ∼4.5[63]). (2) Most of the oxidant species are in their protonated form at this pH, i.e., 91% of the total free chlorine as HOCl (pK_a 7.5[64]) and 98% of the total PAA as protonated PAA (pK_a 8.2[65]), which are more potent oxidants than their respective deprotonated forms. In other words, this pH captures the worst-case scenarios. (3) In our previous study[21] using commercial polyamide membranes, membrane performance and characteristics [via XPS, AFM, and Fourier-transform infrared (FTIR) spectroscopy analyses] were also evaluated at pH 6.5. Using this pH value in the current study has the benefit of maximizing possible comparisons regarding the characterization results. The oxidant solutions were not buffered to prevent the interferences of ionic strength (needed for the buffer capacity) on the swollen nature of the polyamide film.[66,67] The changes in frequency (Δf) and dissipation (ΔD) of the polyamide-coated QCM sensor after exposure to oxidant solutions were recorded at the fundamental frequency (5 MHz) as well as its overtones (from 3 to 13) over the entire course of the measurement.

Atomic Force Microscope (AFM) Measurements. Topographical images and force−displacement curves were obtained on freshly prepared and oxidant-exposed polyamide films using AFM (BioInfinity, Oxford Instrument). Contact mode imaging was conducted to measure the surface morphology and film thickness (scratch-test) of the mLBL polyamide films in dry (ambient air) and wet (DI water) conditions. A sharp-tip AFM cantilever (k_n ∼ 0.2 N m^{-1}, HQ-13-Au, Oxford Instruments) was employed for imaging. The root-mean-square (RMS) roughness of the films was estimated using a 1 × 1 μm^2 image window. The reported values are the average of measurements taken at five different locations *per* sample.

Fast force mapping (FFM) mode was employed to observe polyamide degradation kinetics in the presence of oxidants, which also complemented QCM-D analysis by capturing the polymer film behavior in oxidant solutions under no-flow conditions. In this mode, the force−displacement curves are acquired at a high pixel rate (up to 300 Hz) using a continuous motion of the AFM tip. The maximum indentation force was held at ∼5 nN to observe changes in polyamide film morphology and interaction forces (simultaneously recorded) as the AFM tip (silica) interacts with the polyamide film exposed to the oxidant solution. Temporal variations in adhesion forces and the shape of force profiles were used to infer film heterogeneity and the extent of degradation. FFM measurements were performed inside a liquid cell holding the oxidant solution (100 mg L^{-1} HOCl or 1000 mg L^{-1} PAA, pH 6.5). The polyamide film was pre-swelled in DI water for 2 h before being placed in the oxidant solution. Thermal drifts were minimized during the measurement. For long-duration experiments (e.g., immersion time longer than 2 h), the oxidant solution was periodically added to the liquid cell to account for the solvent evaporation at ambient conditions. A silicon AFM cantilever with a natural oxide coating (k_n ∼ 0.2 N m^{-1}, HQ-13-Au, Oxford Instruments) was employed for FFM measurements. Tip contamination was minimized by intermittently cleaning the tip in ethanol. The deflection sensitivity of the cantilever was estimated by acquiring a force−displacement curve on a clean bare silica wafer. The normal spring constant of the cantilever was calibrated using the thermal noise method.[68] FFM images were collected at a tip approach rate of 75 Hz. It should be noted that the hydrodynamic forces acting on the AFM lever from the surrounding aqueous medium will influence the measured pull-off forces. However, by employing a constant approach rate and using similar AFM tip radii (nominal radius of ∼10 nm) across all measurements, the changes in adhesion forces with polymer degradation can be compared.

X-ray Photoelectron Spectroscopy (XPS) Measurements. The chemical composition of the pristine and oxidant-exposed polyamide films on QCM sensors was determined using an XPS (Scienta Omicron ESCA2SR). Based on the real-time QCM studies, oxidant-exposed polyamide films were collected at different sorptions and degradation stages and were used for XPS analysis. The collected QCM sensors were immediately immersed in a DI water bath to stop the polyamide−oxidant reactions. The survey and high-resolution spectra were collected at 200 and 50 eV pass energies, respectively, using a monochromatic Mg Kα radiation (1253.6 eV). A charge neutralization flood gun was used, and the binding energies were charge-corrected by offsetting the C 1s peak to the standard 284.8 eV. CasaXPS software (version 2.3.22) was used for determining elemental composition analysis and peak-fit analysis. Peak fits for high-resolution spectra of C 1s, N 1s, O 1s, and Cl 2p were made using relative sensitivity factors of 1, 1.8, 2.93, and 2.29, respectively. The U Touguard Poly-type for background subtraction and a Gaussian−Lorentzian signal-type for peak shape were employed. Atomic percentages obtained from XPS analysis were used to calculate the degree of cross-linking for the polyamide films using the following equation[69]

$$\text{crosslink}\ (\%) = \frac{m}{m+n} \times 100 \tag{1}$$

where m and n are the cross-linked and linear parts of the polyamide layer, respectively. The values of m and n can be estimated based on the O/N ratios of the sample.[69−71]

THEORETICAL BASIS

Polymer Mass Change in QCM-D. The frequency change in the thin layer of the polyamide film recorded by the QCM-D is converted to a mass change using Sauerbrey's equation[72]

$$\Delta m = -C\left(\frac{\Delta f}{n}\right) \tag{2}$$

where Δm is the change in the mass coupled with the sensor (ng cm^{-2}), C is a constant dependent on the intrinsic properties of the quartz sensor (C = 17.7 ng cm^{-2} Hz^{-1} for a 5 MHz AT-cut quartz crystal), n is the overtone, and Δf is the change in frequency (Hz). The Δm values calculated using eq 2 represent the changes in the wet mass of the polymer film, which includes both film mass and the associated water molecules within the polymer network.

Modeling Sorption Kinetics of Oxidant-Exposed Polyamide Films. The interactions between the oxidants and polyamide can lead to mass increase of the polyamide film via physical (ad)sorption of the intact oxidant molecules (as HOCl or PAA), absorption of the oxidant molecules in the polymer matrix after diffusion, and chemical reactions between polyamide and the oxidants (e.g., incorporation of the Cl atom

https://doi.org/10.1021/acs.langmuir.1c02835
Langmuir XXXX, XXX, XXX−XXX

Table 1. Summary of the Elemental Composition of Polyamide Thin Films in Pristine Condition and after Treatment with HOCl (100 mg L^{-1}) and PAA (1000 mg L^{-1}) Obtained from XPS Analysis[a]

	atomic composition						
sample	O 1s	C 1s	N 1s	Cl 2p	O/N	Cl/N	cross-link density (%)
pristine	12.68	71.29	9.07	ND[b]	1.40		50
HOCl (sorption)	11.72	73.01	8.02	1.70	1.46	0.21	43.9
HOCl (degradation)	11.52	70.41	7.38	6.89	1.56	0.93	34.4
PAA (degradation)	13.23	74.06	8.36	ND	1.58		32.6

[a]HOCl/PAA-treated samples were collected from QCM experiments at the sorption or degradation phases. [b]ND, not detected.

after *N*-chlorination). The Δm−time profiles of the polyamide films upon oxidant exposure were fit to kinetic models to obtain the sorption rate constants. In these models, Δm refers to the difference between the initial (wet) film mass on the QCM sensor and the film mass upon oxidant exposure at time t. Data fitting was conducted using OriginPro 2018. The sorption kinetics are modeled as follows:

(a) The Boltzmann-sigmoidal model for sorption, also known as the logistic equation, is used to describe scenarios such as autocatalytic reactions,[73] phase transitions,[74] and other interfacial physicochemical interactions.[30,31,75] The model assumes an initial fast (exponential) change in the substrate/film mass and subsequently a slower rate change to approach a plateau. This behavior produces a characteristic *S*-curve described by eq 3.[75] The decreasing sorption rate can be attributed to the gradual saturation of sorption sites or a transition from a sorption-dominated process to a concurrent sorption/degradation process in polyamide transformation

$$\Delta m = A_{b1} + \frac{A_{b2} - A_{b1}}{B + e^{t_i - t/R_{b,s}}} \quad (3)$$

where A_{b1} and A_{b2} are the initial (bottom asymptote) and final (top asymptote) masses of the polyamide film (ng cm^{-2}), respectively, t is the time after the introduction of oxidants (min or h), t_i refers to the time at which the inflection of accumulation rate (maximum dm/dt) occurs (min or h), $R_{b,s}$ is the reciprocal of the sorption rate change (min or h), and B is a parameter to adjust the position of t_i with respect to the geometric location of the point of inflection. For the sorption process, A_{b1} was set to zero (i.e., baseline pristine polyamide film) and B to 1, while magnitudes for A_{b2} and $R_{b,s}$ were estimated from the fits.

(b) The pseudo-first-order model (eq 4) is frequently applied to describe adsorption processes that involve diffusion through an interface.[76−78] It is based on the assumption that the rate of mass change at any given time is proportional to the difference in the maximum sorbable solute mass (i.e., at saturation) and the solute mass present on the surface at time t. Similar to previous studies,[78−80] this model can be employed to characterize the sorption process within the first few minutes after injecting the oxidant solution into the QCM cell

$$\Delta m = A_p(1 - e^{-k_p t}) \quad (4)$$

where A_p is the maximum mass gain (ng cm^{-2}), and k_p is the first-order rate constant (min^{-1}). Both parameters were obtained from data fitting.

Modeling Degradation Kinetics of Oxidant-Exposed Polyamide Films. After the initial mass sorption, the polyamide film shows degradation when exposed to the oxidants, as indicated by the increase in frequency in QCM experiments. The sorption maximum was considered as the onset of the degradation-dominated process. In the degradation kinetics models, Δm refers to the difference between the initial wet mass of the polyamide film and the mass at a given time in the degradation phase. The time corresponding to the sorption maximum was set to zero for model fitting. The desorption kinetics are modeled as follows:

(a) The two-step exponential model (eq 5) describes the degradation processes that have two reaction rates[80]

$$\Delta m = m_e + A_{t1}\, e^{-k_{t1}t} + A_{t2}\, e^{-k_{t2}t} \quad (5)$$

where m_e is the final equilibrium mass left on the QCM sensor (ng cm^{-2}), A_{t1} and A_{t2} are the pre-exponential terms (ng cm^{-2}), and k_{t1} and k_{t2} are the rate constants (h^{-1}). The pre-exponential terms and the rate constants were obtained from the fits.

(b) The Boltzmann-sigmoidal model (eq 6) has been used to describe degradation processes initiated by the sorption of a chemical stimulus, as observed in the enzymatic degradation of film and can be described as[30−33]

$$\Delta m = A_{b3} + \frac{(A_{b4} - A_{b3})}{B + e^{t_i - t/R_{b,d}}} \quad (6)$$

where A_{b3} and A_{b4} (ng cm^{-2}) are the masses at the onset of degradation and when degradation equilibrium is reached, respectively, t is the time after sorption maximum (h), and t_i refers to the time at which the inflection of degradation rate (maximum $|dm/dt|$) occurs (h). The value for $R_{b,s}$ represents the reciprocal of the degradation rate change (h), and B is as defined for eq 3 and obtained from the fit.

RESULTS AND DISCUSSION

Characterization of Dry Polyamide Films on Silica Substrates. AFM topography measurements estimated the dry-film thickness of the 15-bilayer polyamide film deposited on the silica wafer to be 17.0 ± 1.8 nm (average from three replicates, with one of the replicates shown in Figure S1). These values correspond to a film growth rate of approximately 1.1 nm per cycle of mLBL deposition (i.e., a bilayer of TMC and MPD) and are consistent with the values reported elsewhere (average 0.9 nm and maximum 1.2 nm per cycle).[53] The surface roughness of the dry film measured on six replicate samples was consistently found to be low (1.3 ± 0.5 nm), indicating that the film was relatively smooth and the synthesis

https://doi.org/10.1021/acs.langmuir.1c02835
Langmuir XXXX, XXX, XXX−XXX

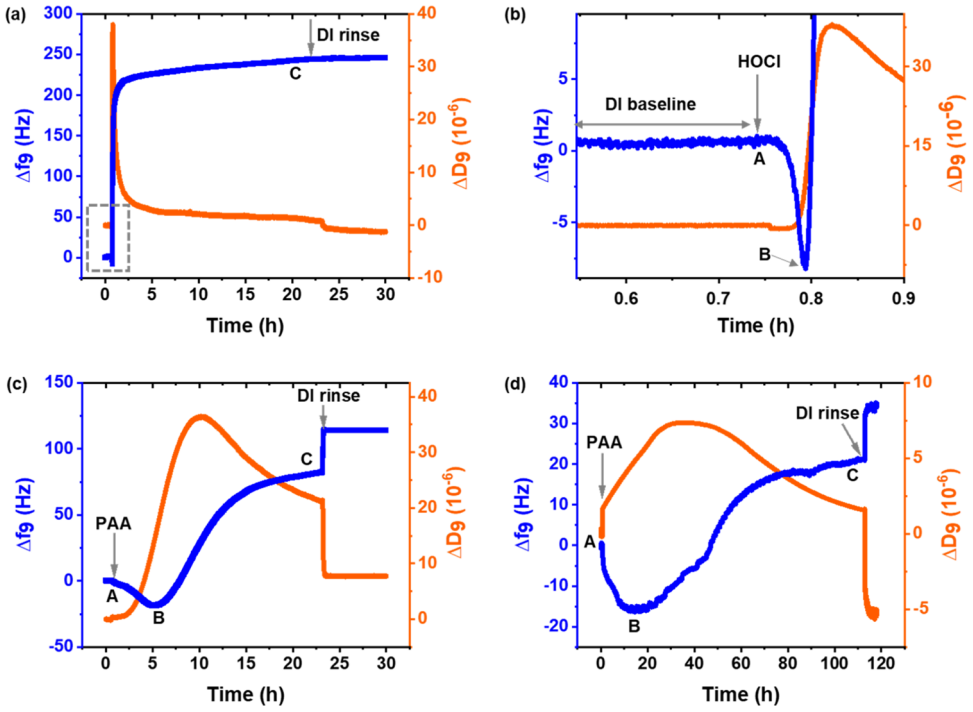

Figure 1. Δf and ΔD responses of the polyamide films (9th overtone) when exposed to (a, b)100 mg L^{-1} HOCl, (c) 1000 mg L^{-1} PAA (fast kinetics), and (d) 1000 mg L^{-1} PAA (slow kinetics). The initial Δf and ΔD responses upon exposure to HOCl (dashed box in panel (a)) is shown in panel (b). Points A–C on the Δf–time curves correspond to oxidant introduction, maximum oxidant sorption, and equilibrium after degradation, respectively. The characteristic times and frequency changes at these points are summarized in Tables S1 and S2. Representative Δf and ΔD responses of the polyamide film across different overtones (n = 3–11) for the PAA fast kinetics experiment are shown in Figure S2a.

was reproducible. By measuring the frequency difference of bare and polyamide-coated QCM sensors (9th overtone), the dry polyamide film mass was estimated as 3501 ± 727 ng cm^{-2} (eight replicates), which is comparable with the reported value for the polyamide films synthesized by a similar mLbL method (3600 ng cm^{-2}).[48] The variability of the dry-film mass is likely attributed to the occasional polymer accumulation on the backside of the QCM sensor during the spin-coating process despite the cleaning steps. However, this variability is not expected to affect the kinetic measurements. The final annealing step in the polyamide film synthesis protocol showed no impact on the surface roughness of the film but significantly improved its attachment to the QCM sensor, preventing delamination of the film under DI water flow across the QCM sensor.

XPS analysis of the as-prepared polyamide film showed an O/N ratio of 1.4 (Table 1), indicating a 50% cross-link (O/N ratio of 1 for fully cross-linked and 2 for entirely linear polyamide films).[81] The cross-link percentage of mLBL polyamide films is similar to the commercial NF90[82] and FT-30 Filmtec[83] nanofiltration/reverse osmosis membranes.

Oxidative Degradation of Polyamide Films under Flow Conditions. *Comparing HOCl- and PAA-Induced Polyamide Degradation Time Profiles.* QCM-D was used to examine the degradation of polyamide films when exposed to oxidants under flow conditions (50 μL min^{-1}). The polyamide film was initially equilibrated in DI water for at least 2 h to achieve a stable baseline (i.e., Δf < 1 Hz for at least 20 min). The wet mass of the polyamide film was estimated as 8466 ± 979 ng cm^{-2} (based on the frequency difference between bare and polyamide-coated sensors in DI; eight replicates), corresponding to a film hydration of 48.7 ± 8.0%. This value is significantly smaller than those measured for hydrated polymer brushes[84] and other hydrogels,[85] indicating the high density of the mLBL polyamide film.

Two control experiments were conducted to evaluate the potential effects of density and ionic strength of the solutions on the observed frequency and dissipation changes. First, Δf and ΔD for a bare crystal upon exchange from DI water to an oxidant solution (100 mg L^{-1} HOCl or 1000 mg L^{-1} PAA) were recorded. Second, Δf and ΔD for polyamide-coated QCM sensors when the solution was exchanged from DI water to a saline solution (1.4 mM NaCl or 32 mM NaAc, simulating the ionic strength of 100 mg L^{-1} HOCl or 1000 mg L^{-1} PAA, respectively) were measured. In both cases, Δf < 2 Hz and ΔD < 2 × 10^{-6} were measured, confirming that the Δf and ΔD observed in HOCl/PAA experiments originate from the interactions between the polyamide film and the oxidants.

HOCl Experiments. Figure 1a shows the representative time profiles of Δf (left axis) and ΔD (right axis) when the polyamide film was exposed to 100 mg L^{-1} HOCl solution for ~24 h. The Δf and ΔD changes immediately after HOCl introduction are replotted in Figure 1b. After the addition of HOCl (point A in Figure 1b), the frequency of the QCM sensor decreases sharply with a simultaneous increase in dissipation, indicating mass sorption in the polyamide film. Beyond a maximum frequency drop (point B), the frequency starts to increase, indicating polyamide film degradation, until an equilibrium value is achieved (point C; Figure 1a). The maximum frequency drop (i.e., sorption maximum at point B) after HOCl exposure was 13.9 ± 5.2 Hz (four replicates; Table S1 and Figure S2b) and occurred within the first 2.3 ± 0.9 min. At point B, the increase in film mass was estimated as 246 ± 92 ng cm^{-2} (eq 2). At degradation equilibrium (point C), the net

https://doi.org/10.1021/acs.langmuir.1c02835
Langmuir XXXX, XXX, XXX–XXX

frequency increase from the intact wet film was obtained as 283 ± 40 Hz (Table S1), corresponding to a 43.7 ± 7.3% loss of the initial wet mass from the surface. The time required for the polyamide film to reach this equilibrium varied between 6 and 20 h. No further frequency change was observed after the DI water rinse step at the end of the experiments.

The Δf−time profiles are consistent with the polyamide−chlorine reaction pathways proposed in previous studies, i.e., chlorine first attacks the amide bond (i.e., *N*-chlorination), leading to the hydrolysis of the amide bonds and/or ring chlorination via Orton rearrangement.[50,51,86] This pathway can also explain the absence of sorption equilibrium in our experiments, as there is simultaneous incorporation of Cl atoms and breakage of the amide bonds within the film. The incorporation of Cl atoms into the polyamide network is also supported by our XPS analyses (Table 1). In contrast to the absence of Cl signals in the as-prepared film, the Cl/N ratios of the samples collected at the sorption and degradation stages showed values of 0.21 and 0.93, respectively. High-resolution spectra provide further evidence to support the reaction pathway (Figure S3). For example, the sample collected at the initial sorption phase showed an upward shift of the N 1s peak (by 0.25 eV) compared to the as-prepared film, suggesting a more electronegative environment from *N*-chlorination.[48] In contrast, no such shift (∼0.06 eV) was observed for the sample collected at the degradation phase, consistent with the short-lived nature of the *N*-chlorinated intermediates.[48,87] Further, the binding energies for Cl $2p_{3/2}$ peaks were obtained at ∼197.4 and ∼200.6 eV for both sorption and degradation samples, respectively. The latter peak (200.6 eV) can be attributed to the formation of structures similar to 2-chlorostyrene.[48,88] Additionally, the area under this peak increased from 52% in the sorption-phase sample to 63% in the degradation-phase sample. The relatively high percentage of organic chlorine in the sorption stage indicates the simultaneous occurrence of *N*- and ring chlorination reactions in polyamide.

The sorption−degradation behavior of polyamide in HOCl follows similar trends reported in a recent QCM study by Kearney and Howarter,[48] except our measurements show single-stage chlorine (ad)sorption process than the reported two-stage behavior. This difference may arise from two factors. First, Kearney and Howarter used chlorine solutions at pH 7.4,[48] while our experiments were conducted at pH 6.5. With a pK_a of 7.5,[64] more than 90% of the total free chlorine is in the form of hypochlorous acid (HOCl) at pH 6.5, whereas HOCl and hypochlorite (OCl^-) each account for roughly half of the total free chlorine at pH 7.4. A recent study using benzanilide-based compounds showed that OCl^- is more reactive than HOCl in *N*-chlorination, but HOCl is more reactive during in-ring chlorination.[21] Second, we used a slower flow rate (50 μL min^{-1}) than that employed by Kearney and Howarter (150 μL min^{-1}).[48] Slower flow rate allows for an increased interaction time between the solute and surface, which may facilitate in-ring chlorination reaction. In line with the XPS measurements, the single-stage sorption process indicates the simultaneous *N*-chlorination and in-ring chlorination reactions occurring within the film upon exposure to chlorine.

PAA Experiments. Figure 1c,d represents QCM measurements for the polyamide films exposed to 1000 mg L^{-1} PAA solutions. Note that the concentration used for PAA measurements is 10 times higher than that used for HOCl measurements. The higher concentrations for PAA were necessary to measure observable physicochemical changes in the film and within a reasonable experimental time frame (minimum drift). Because we initially observed divergence in the PAA-induced polyamide degradation behavior under fully controlled conditions, we conducted a total of eight experiments. As shown in Table S1, four of these experiments showed relatively fast kinetics, reaching the sorption maximum (point B) after 4.6 ± 1.7 h (Figure 1c), while the others showed relatively slow kinetics, reaching the sorption maximum only after 20.5 ± 9.2 h (Figure 1d). The maximum frequency drop at the end of the sorption process was not significantly different between experiments exhibiting fast and slow kinetics (22 ± 5 and 19 ± 5 Hz, respectively), corresponding to a mass gain of 361 ± 92 ng cm^{-2} (eq 2). Once attaining the sorption maximum (point B), the degradation equilibrium (point C) was reached after 7−30 h (fast) and 60−96 h (slow) (Table S1). Based on the net frequency changes at degradation equilibrium, the polyamide films lost 28 ± 16% of the initial wet mass. After achieving the degradation equilibrium (point C), the oxidant solution in the QCM cell was exchanged with DI water. An additional increase in frequency was observed (Figure 1c,d), suggesting the presence of loosely attached polymer chains in PAA-exposed polyamide films, even after achieving degradation equilibrium.

Compared with chlorine, much less is known about the interaction mechanisms of PAA with polyamide. Given the lower reactivity of PAA with polyamide than HOCl,[21] it is expected that the physical sorption of PAA could occur before any chemical changes in the polyamide film. In addition, as PAA does not solely target the amide bond, as indicated by the product analysis of the reaction between PAA and benzanilide (a model aromatic amide),[21] PAA may induce chemical changes to the polyamide film that do not result in an immediate and rapid disruption of the polymer network. Both these phenomena are consistent with the gradual decrease in frequency during the sorption phase of PAA experiments. In the degradation phase, oxygen incorporation on the polyamide film was observed based on the XPS analysis (Table 1). The O/N ratio showed an increase from 1.40 for the as-prepared film to 1.58 for the PAA-treated film. A recent study using commercial nanofiltration membranes reported similar results and proposed the new oxygen-containing functional groups to be carboxylic, hydroxyl, and epoxide groups based on Fourier-transform infrared (FTIR) spectroscopy analysis and model amide compound experiments.[21] We also attempted FTIR-attenuated total reflectance (ATR) analysis on the polyamide thin films (<20 nm) in this study, but due to a low signal-to-noise ratio (SNR) of the spectra,[89] this approach was not continued. Our high-resolution XPS spectra of the O 1s region showed that the PAA-exposed polyamide film (degradation phase) had a negative shift (0.5 eV) of the C═O peak from the as-prepared film, which may be attributed to the formation of benzoquinone-like structures (Figure S4).[90,91] A future study using angle-resolved XPS to achieve time- and depth-resolved measurements is warranted to further elucidate the PAA-induced chemical transformations of polyamide films.

Comparison of HOCl- and PAA-Exposed Films. The mass gain of the polyamide films at the sorption maximum (point B) in PAA experiments (361 ± 92 ng cm^{-2}) was slightly higher than that in HOCl experiments (246 ± 92 ng cm^{-2}). However, HOCl-exposed films reached sorption maximum (<5 min) substantially faster than PAA-exposed films (3−7 h for fast kinetics), confirming the greater reactivity of HOCl with

https://doi.org/10.1021/acs.langmuir.1c02835
Langmuir XXXX, XXX, XXX−XXX

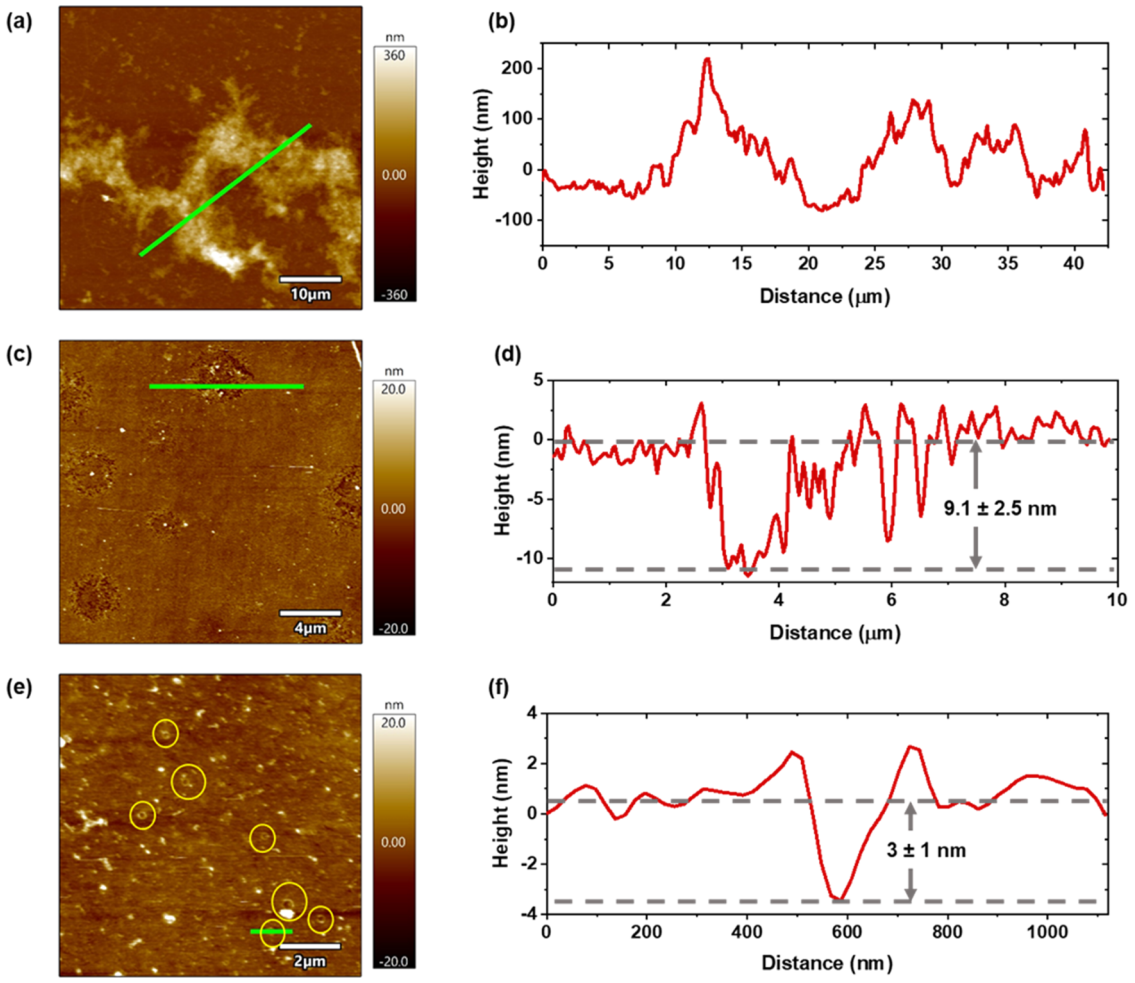

Figure 2. AFM images of the polyamide-coated QCM sensors measured at the end of oxidant exposure QCM experiments: (a) 100 mg L^{-1} HOCl, (c) 1000 mg L^{-1} PAA (fast kinetics), and (e) 1000 mg L^{-1} PAA (slow kinetics). Circles in panel (e) mark the positions of the small pits. The section profiles in panels (b, d, f) correspond to the green lines on the AFM images in panels (a, c, e), respectively. Error bars in panels (d, f) are calculated from measurements across multiple pits on the same sample.

polyamide than that of PAA. Additionally, PAA-exposed films lost less initial mass than HOCl-exposed films by the time degradation equilibrium was achieved (27.8 ± 15.6 and 43.7 ± 7.3% of the initial wet mass, respectively).

An examination of the Δf−time profiles at different overtones in PAA experiments showed that the maximum frequency drop (corresponding to the sorption maximum) between overtones occurred at distinct time points, i.e., an offset of 20−30 min was observed between n = 7 and 11 overtones (fast kinetics) (Figure S5). Similar offsets were also observed for PAA slow kinetic experiments. The decay lengths of the acoustic wave generated by the quartz crystal at these overtones range from ∼95 to 70 nm (in DI water, 20 °C) and are comparable to the wet thickness of the polyamide film (80 nm). Hence, this overtone-dependent sorption maximum indicates heterogeneous (de)sorption processes along the thickness of the film. The delayed arrival of the maximum frequency drop for lower overtones suggests continued transformations in the polyamide network (e.g., hydroxylated rings with intact amide bonds) occurring near the liquid−film interface. Further, oxidant-induced morphological changes occurring at the liquid−film interface (shown using AFM in Figure 2) also suggest continued incorporation of water/PAA molecules at the interface than deep within the dense polyamide network, leading to the observed overtone-dependent behavior. In contrast, a minimal offset was observed in HOCl experiments (<0.6 min), attributable to the rapid disintegration of the polymer network via amide bond cleavage.

In both HOCl and PAA experiments, the dissipation signal of the polyamide films increased almost instantaneously upon introducing the oxidant (Figure 1), suggesting that the initial oxidant−polyamide interaction rendered the film more prone to hydration. In HOCl experiments, the maximum dissipation was reached very close to the sorption maximum (point B, Figure S2b; Table S2). Beyond this, the decrease in dissipation accompanied the increase in frequency, indicating both polymer and associated hydration mass losses during the degradation process. In contrast, the PAA experiments showed a continued increase in dissipation for several hours despite increasing frequency after the sorption maximum (Figure S5 and Table S2). This behavior is consistent with the PAA−polyamide interaction mechanism proposed above: some of the polymer mass starts to detach from the surface polyamide layers due to amide bond breakage (frequency increase); however, other transformations within the polyamide network (e.g., ring oxidation) continue to increase film hydration but not cleaving the polyamide network (dissipation increase). The

https://doi.org/10.1021/acs.langmuir.1c02835
Langmuir XXXX, XXX, XXX−XXX

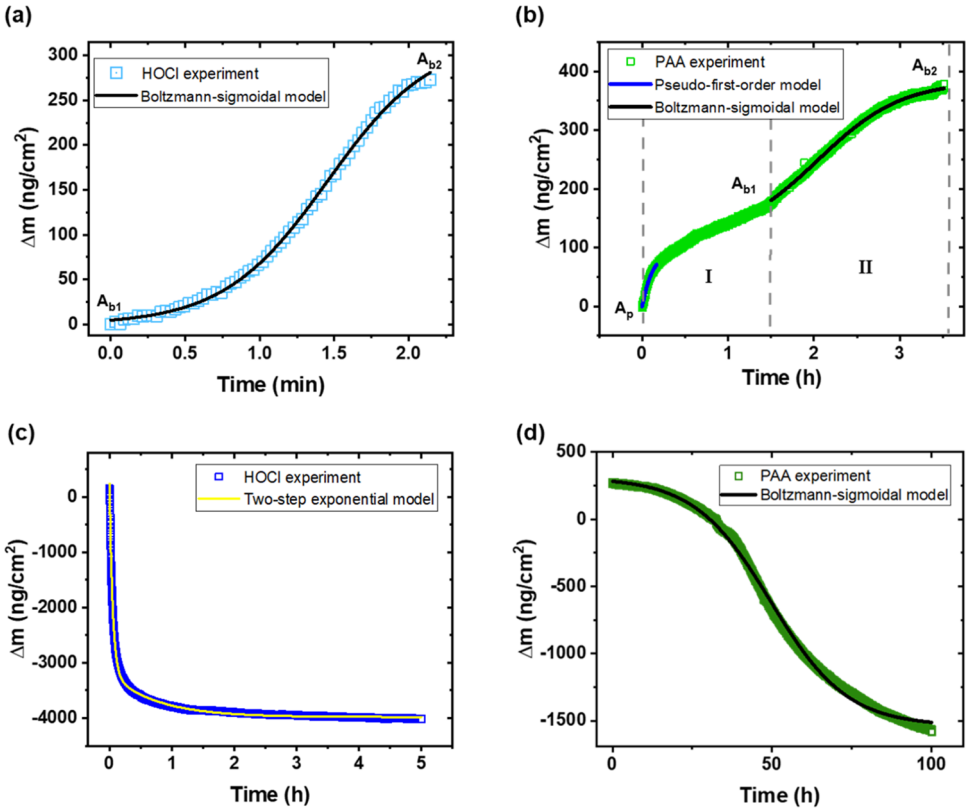

Figure 3. Representative sorption profiles and kinetic model fits for (a) HOCl- and (b) PAA-exposed polyamide films. Representative degradation profiles and kinetic model fits for (c) HOCl- and (d) PAA-exposed polyamide films. For panels (c) and (d), the time of the sorption maximum (point B in Figure 1) was set to zero as the beginning of the degradation-dominant phase. The kinetic parameters are summarized in Tables 2 and 3, with individual replicates shown in Tables S3 and S4.

subsequent decrease in dissipation and the increase in frequency suggest that a rigid film remained when the degradation equilibrium was reached.

To observe the morphological changes in the polyamide film due to oxidant-induced degradation, polyamide-coated QCM sensors were collected at the end of the QCM measurement, air-dried, and imaged by AFM (Figure 2). HOCl-exposed polyamide films (Figure 2a,b) featured pile-ups of >100 nm thickness, much greater than the thickness of as-prepared polyamide films (~17 nm). Additional images showed that certain sections of the polyamide film were peeled off, exposing the underlying substrate (Figure S6a). In contrast, the PAA-exposed film showed minor damage (Figure S6b). Higher-magnification AFM images showed the formation of nano-sized pits across the film (Figure 2c,e). Films exhibiting fast kinetics had larger pits with depths of 9.1 ± 2.5 nm (Figure 2d), whereas those exhibiting slow kinetics featured smaller and shallower pits (depth 3 ± 1 nm; Figure 2f). These results also suggest that the variable kinetics observed in PAA experiments may be attributed to the presence of initial defects in as-prepared films (e.g., the presence of pinholes, cracks, etc.). The presence of pits at the interface of PAA-exposed films, as suggested above, also explains the continued dissipation past the sorption maximum. The pits, once formed, can increase the film roughness and thereby enhance the friction dissipation of entrapped water molecules associated with the polymer film.[92−94] Only after a substantial amount of film is removed from the surface, the effects of roughness on ΔD could be overcome.

Kinetic Modeling of HOCl- and PAA-Induced Polyamide Degradation. The kinetic parameters of the oxidant-induced sorption and degradation processes in the polyamide film were obtained by fitting the Δm−time curves to the selected models described in the Theoretical Basis section. In this study, Δm was calculated using Sauerbrey's equation (eq 2), which assumes that the film is rigidly bound to the sensor and has density and stiffness comparable to the underlying sensor (i.e., $\Delta D < 2.0 \times 10^{-6}$).[95−98] Although a significant portion of our QCM data showed $\Delta D > 2.0 \times 10^{-6}$, an approximation with Sauerbrey's equation is made to focus on the study to compare kinetic constants for HOCl- and PAA-induced polyamide degradation. A few previous studies employed Sauerbrey's approximation in cases of high ΔD for the kinetic modeling of enzymatic degradation of milk proteins[99] and polymers[35] and for understanding the swelling behavior of proteins and obtaining sorption isotherms of proteins on nanogels[38] and self-assembled monolayers.[100] We made attempts to use the standard Voigt model to obtain the film's wet mass, but they were hampered by the poor fits resulting from the unknown (heterogeneous) film density, the extremely rapid frequency changes in HOCl experiments (insufficient resolution by the QCM instrument), and the observed offsets for the maximum frequency drops among different overtones. As shown in Figure S5 for a representative PAA fast kinetic sample, the time for the maximum frequency drop to occur increased from 3.5 h for $n = 9$ to 5 h for $n = 7$. This suggests that a density gradient developed along the depth of the film as it started to degrade. Accordingly, a carefully designed multilayer viscoelastic model would be

https://doi.org/10.1021/acs.langmuir.1c02835
Langmuir XXXX, XXX, XXX−XXX

Table 2. Average Kinetic Fitting Parameters for HOCl Experiments[a]

sorption phase				degradation phase			
Boltzmann-Sigmoidal model $\Delta m = A_{b1} + \frac{A_{b2} - A_{b1}}{1 + e^{t_i - t/R_{b,s}}}$				two-step exponential function $\Delta m = m_e + A_{t1}\, e^{-k_{t1}t} + A_{t2}\, e^{-k_{t2}t}$			
A_{b2} (ng cm^{-2})	t_i (min)	$R_{b,s}$ (min)	m_e (ng cm^{-2})	A_{t1} (ng cm^{-2})	k_{t1} (h^{-1})	A_{t2} (ng cm^{-2})	k_{t2} (h^{-1})
324 ± 163	1.7 ± 0.2	0.4 ± 0.1	−6331 ± 3450	4992 ± 2201	16.3 ± 12.2	1625 ± 1213	0.12 ± 0.06

[a]The fitting parameters for individual experimental runs are shown in Tables S3. Details on the kinetic models and data fitting are shown in the Theoretical Basis section.

needed along with independent measurements to fully capture the mass change during the degradation process. It is beyond the scope of this work and can be pursued in future studies. In this study, the comparison of rate constants between PAA and HOCl experiments is a main focus, and the accuracy of the Δf to Δm model will generate a similar error for both the cases.

Figure 3 shows the representative Δm−time curves and model fitting for the sorption and degradation profiles of HOCl and PAA experiments. The experimental replicates are shown in Figure S7, Tables S3 and S4. For the HOCl experiment, the Boltzmann-sigmoidal model (eq 3) was employed to model the sorption phase (Figure 3a), capturing the increasing influence of film degradation toward the end of the sorption phase. This model was also used in a previous QCM study of HOCl-induced polyamide degradation.[48] As shown in Table 2, the t_i and $R_{b,s}$ values obtained from the HOCl experiments were 1.7 ± 0.2 and 0.40 ± 0.1 min, respectively.

The sorption phase of the PAA-exposed films showed a two-stage behavior (Figure 3b): stage I sorption initially followed a pseudo-first-order model (the first ∼10 min; eq 4), while stage II sorption followed the Boltzmann-sigmoidal kinetics (eq 3). As shown in Table 3, all PAA experiments had similar pseudo-first-order rate constants (k_p) in the initial stage I sorption (0.20 ± 0.07 and 0.17 ± 0.04 min^{-1} for fast and slow kinetics, respectively); in stage II sorption, however, the experiments with slow kinetics had 4 times greater Boltzmann-sigmoidal $R_{b,s}$ values (2.05 ± 0.21 h) than those with fast kinetics (0.55 ± 0.16 h). The two-stage sorption process in PAA experiments may be explained by the initial physical sorption of PAA molecules on the polyamide surface in stage I (independent of the initial state of the film) and the subsequent diffusion of PAA and its reaction with the polyamide network in stage II. The dependence of the latter step on the initial film defects leads to the variability in the sorption kinetics of PAA-exposed polyamide films. The different sorption mechanisms of HOCl- and PAA-exposed films render it difficult to draw simple comparisons based on the kinetic parameters. However, it can be estimated that PAA is at least 50 times less reactive than HOCl with polyamide based on the comparison of the sorption phase $R_{b,s}$ values between HOCl experiments (0.40 ± 0.1 min) and the stage II in PAA experiments (0.55 ± 0.16 h, fast kinetics).

Figure 3c,d shows the representative degradation profiles of HOCl- and PAA-exposed polyamide films, respectively, and the corresponding model fits. The degradation of polyamide films by HOCl followed a two-step exponential model (eq 5). As shown in Table 2, the film mass rapidly decreased after sorption maximum (k_{t1} = 16.3 ± 12 h^{-1}), suggesting that the polyamide film was partially delaminated. The subsequent slower degradation (k_{t2} = 0.12 ± 0.06 h^{-1}) likely corresponds to the continuous disintegration of the remaining polyamide film. In comparison, PAA-mediated degradation did not show a rapid mass loss immediately after sorption maximum but instead followed the Boltzmann-sigmoidal kinetics (eq 6) with a gradual start of mass loss. This suggests that PAA exposure did not lead to delamination or peeling-off of the film, consistent with the AFM topographical measurements (Figures 2 and S6). The slow initiation of film degradation by PAA, in contrast to that by HOCl, may be attributed to PAA's lower selective reactivity with the amide bond than HOCl, as suggested by model aromatic amide experiments.[21] PAA may first react with the aromatic moieties in polyamide that do not result in the breakage of polymer chains; film degradation (i.e., mass loss) is only detected when amide bonds start to degrade. Experiments with fast and slow kinetics featured $R_{b,d}$ values differing by 5.5-fold (Table S4). Similarly, the time to reach maximum degradation rate (from point B), t_i, is about ∼7.5 times shorter for fast kinetics than for slow kinetics PAA experiments.

A comparison of the degradation profiles for different replicates in HOCl and PAA experiments is shown in Figure S7d. Overall, the degradation profiles of each oxidant exhibit much greater variability than their corresponding sorption profiles among films exposed to the same oxidant. For example, $R_{b,d}$ in PAA experiments (fast) and k_{t2} in HOCl experiments varied by a factor of 3−8 and 1.1−2.5, respectively, whereas k_p in PAA experiments (fast) and $R_{b,s}$ in HOCl experiments varied by 1.25−2 and 1.2−1.4, respectively (Tables S3 and S4). Additionally, there was higher variability in the degradation equilibrium mass for PAA-exposed films (∼50%) than that of their sorption maximum mass (∼25%). The stochastic behavior during the disintegration of polyamide films may be rationalized by the interrelated microscopic processes of oxidant diffusion through the polyamide network and the oxidant−polyamide chemical reactions. The oxidative damage of the polyamide film can create different defects (e.g., pits and cracks) with varying permeability and accessibility to the oxidants; the differential penetration of the oxidants through these defects, in turn, leads to divergent damage on the polyamide film.

Oxidative Polyamide Degradation under No-Flow Conditions. To complement the findings from QCM flow experiments, the morphological changes in the polyamide film in a reservoir of oxidant solution (no-flow) were measured using the FFM mode of AFM. The topography images of the film as a function of immersion time in the oxidant solution are shown in Figure 4a−h. The HOCl-exposed film showed evolving features with increasing immersion times, whereas the PAA-exposed film had no visible changes over time. After 1 h of HOCl exposure, the film showed signs of pitting (arrows in Figure 4a). Further HOCl exposure formed cracks and bubbles (Figure 4b,c). The cracks likely created diffusion pathways for HOCl and water to penetrate deeper into the polyamide film,

https://doi.org/10.1021/acs.langmuir.1c02835
Langmuir XXXX, XXX, XXX−XXX

Table 3. PAA Sorption Showing Fit Parameters by Pseudo-First-Order Model (Stage I, First 10 min) and Boltzmann-Sigmoidal Model (Stage II, Full) and PAA Degradation by Boltzmann-Sigmoidal Model[a]

	sorption phase							degradation phase			
	Pseudo-first-order model (stage I) $\Delta m = A_p(1 - e^{-k_p t})$				Boltzmann-Sigmoidal model (stage II) $\Delta m = A_{b1} + \frac{A_{b2} - A_{b1}}{1 + e^{(t_i - t)/R_{b,s}}}$			Boltzmann-Sigmoidal model $\Delta m = A_{b3} + \frac{(A_{b4} - A_{b3})}{B + e^{(t_i - t)/R_{b,d}}}$			
	A_p (ng cm^{-2})	k_p (min^{-1})	A_{b1} (ng cm^{-2})	A_{b2} (ng cm^{-2})	t_i (h)	$R_{b,s}$ (h)	A_{b3} (ng cm^{-2})	A_{b4} (ng cm^{-2})	B	t_i (h)	$R_{b,d}$ (h)
[b]	92 ± 32	0.2 ± 0.07	163 ± 78	437 ± 143	2.6 ± 0.4	0.55 ± 0.16	478 ± 147	−3286 ± 1631	0.86 ± 0.095	4.1 ± 2	1.7 ± 1.3
[c]	89 ± 28	0.17 ± 0.04	179 ± 139	351 ± 79	4.8 ± 1.9	2.05 ± 0.21	365 ± 85	−1821 ± 824	0.95 ± 0.04	36.4 ± 12.7	9.4 ± 1.8

[a]The value of A_{b3} was constrained to ±10% of the mass at sorption maximum. The rest of the parameters were obtained from data fitting. The fitting parameters for individual experimental runs are shown in Table S4. [b]PAA fast kinetics experiments. [c]PAA slow kinetics experiments.

and the etching of the inner layers of the film could lead to the formation of subsurface bubbles. Over time, these bubbles grew and merged upon further HOCl diffusion and reactions, resulting in bulging features (arrow in Figure 4d), which eventually lead to film delamination. The AFM−FFM analysis also shows that, within the first hour of HOCl exposure, the surface roughness of the film increases by 10 times to 9.5 nm; the roughness continues to increase to 22.4 nm by the end of 9 h (Figure S8), consistent with the increase in heterogeneity as the polyamide film degraded (Figure 2a). After 10 h, the film could no longer be imaged, as it was delaminated from the silica wafer even at the slightest application of force while imaging. In contrast, in the PAA solution, no visible changes in the film morphology were observed even after 79 h of exposure (Figure 4e−h); a small (∼2-fold) increase in surface roughness was observed only after 148 h of exposure (Figure S8). PAA exposure induced pit formation on the polyamide film in QCM experiments (Figure 2c,d) but did not alter film morphology in a stagnant PAA solution (Figure 4e−h), highlighting the importance of flow-derived shear force in the degradation kinetics of polyamide films.

In addition to topography images, the AFM−FFM mode also generated force maps for the as-prepared and oxidant-exposed films (in stagnant oxidant solutions). The histograms of pull-off forces between the silica AFM tip and the films are distinct between HOCl and PAA experiments (Figure 4i). The HOCl-exposed film showed a multimodal distribution in the histograms, as well as an overall increase in the pull-off forces over time. For example, the pull-off force histogram after a 1 h HOCl exposure showed four peaks, with the highest frequency peak at 2.4 ± 0.2 nN, and after 13 h, the highest frequency peak shifted to 13.8 ± 0.6 nN. The multimodal distribution of pull-off forces with high standard deviation indicates the spatial heterogeneity of the HOCl-exposed polyamide film. Moreover, a high percentage of individual force−displacement curves showed multiple rupture events when the tip was retracted from the surface (shown in Figure S9a), indicating uncoiling and detachment of the loosely attached polymer chains when the tip is withdrawn from the surface.

In contrast, the histograms of pull-off forces for the PAA-exposed film show a narrow Gaussian distribution (Figure 4i), with the mean pull-off forces decreasing with immersion time (Figure S9b). The mean pull-off force after a 1 h PAA exposure was 1.3 ± 0.2 nN, similar to that measured in DI water (1.75 ± 0.4 nN); after 148 h, the force decreased to 0.25 ± 0.06 nN. The individual force−displacement curves from the PAA experiment predominantly represented electrostatic repulsion (Figure S9c), even after 148 h of PAA exposure. The repulsion interaction is consistent with the negative charges on both the polyamide film (isoelectric point of ∼4.5)[63] and the AFM tip (with natural silica oxide; isoelectric point of ∼2)[101] at the experimental pH (6.5), further suggesting the stability of the polyamide film in the stagnant PAA solution.

CONCLUSIONS

This study utilized QCM-D and other complementary tools (XPS, AFM−FFM) to provide mechanistic insights into PAA−polyamide interactions. In comparison with the conventional disinfectant HOCl, PAA similarly displayed a sorption phase and then a degradation phase in QCM-D experiments. However, the sorption phase in PAA experiments was much longer (3−34 h) than that in HOCl experiments (1.4−3.5 min). PAA experiments also showed a two-stage kinetics

https://doi.org/10.1021/acs.langmuir.1c02835
Langmuir XXXX, XXX, XXX−XXX

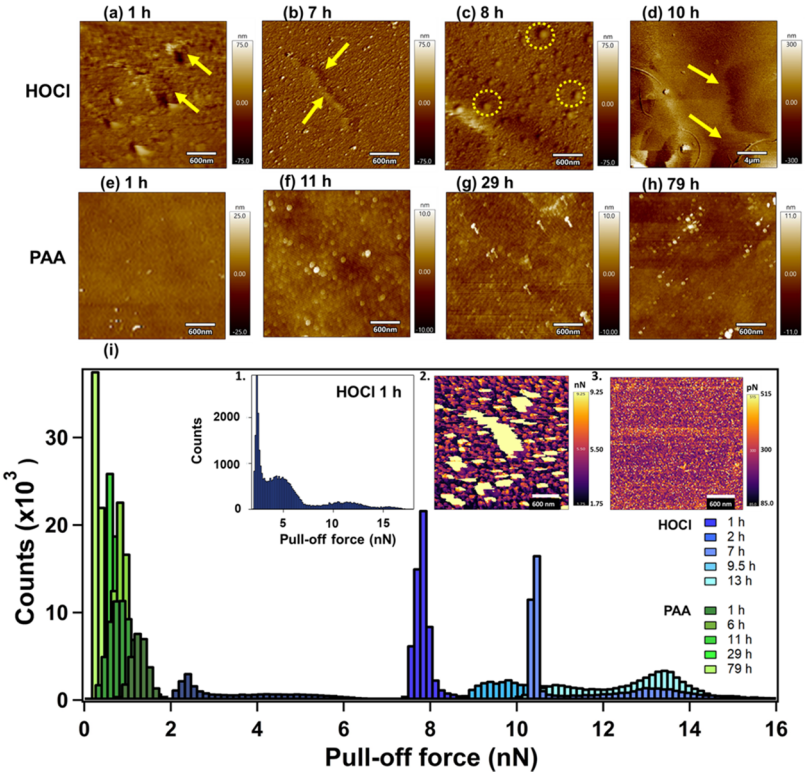

Figure 4. FFM images of the polyamide films immersed in (a–d) 100 mg L^{-1} HOCl, with features highlighted with arrows or circles, and (e–h) 1000 mg L^{-1} PAA, showing no significant change over time. (i) Distribution of the pull-off forces between the AFM tip and the polyamide film immersed in HOCl (blue bars) or PAA (green bars). Inset 1 is a zoomed-in view of the pull-off force histogram in HOCl after 1 h. Insets 2 and 3 show the force maps for polyamide films after 1 h in HOCl and 79 h in PAA, respectively.

within its sorption phase, which followed pseudo-first-order and Boltzmann-sigmoidal models, respectively. Of the total eight PAA experimental replicates, all had consistent kinetic constants in stage I but showed a 4-fold difference in stage II, suggesting a process involving a consistent initial physical sorption of PAA and subsequently a more stochastic PAA diffusion and oxidation of polyamide. At degradation equilibrium, the total (wet) mass loss of the PAA-exposed film was 36% less than that of the HOCl-exposed films. AFM imaging of the polyamide film at the end of the QCM experiments revealed film detachment from the substrate by HOCl exposure and only pitting/wrinkling by PAA. XPS confirmed oxygen incorporation on the PAA-exposed film. AFM–FFM was used for the first time to examine polyamide degradation by oxidants. Under no-flow conditions, force maps of the PAA-exposed films showed minimal change with exposure as long as 148 h, whereas the pull-off forces for HOCl-exposed films increased substantially over time and showed a multimodal distribution, suggesting the evolution of spatial heterogeneity. We also observed that the effects of PAA on polyamide were much smaller in a stagnant solution (AFM) than under constant shear flow (QCM-D).

Overall, our study demonstrated the greater compatibility of polyamide with PAA than with HOCl and that QCM-D can be a useful technique to examine polyamide degradation by oxidants. Future studies can further investigate the PAA–polyamide interaction using strategies such as varying initial PAA concentrations and incorporating depth-resolved surface chemical analysis (e.g., by angle-resolved XPS[49,102]). Additional considerations may also be given to correlating the polyamide transformation measured by QCM-D with the change in the polyamide membrane surface.

■ ASSOCIATED CONTENT

Supporting Information

The Supporting Information is available free of charge at https://pubs.acs.org/doi/10.1021/acs.langmuir.1c02835.

AFM images of as-prepared polyamide film, schematic of characteristic Δf–time curve of a typical QCM experiment, XPS high-resolution N 1s and Cl 2p spectra, Δf and ΔD vs time profiles across multiple overtones, AFM images of the degraded polyamide film at the end of QCM experiments, replicates of sorption and degradation profiles for HOCl and PAA, roughness of a polyamide film as a function of HOCl/PAA exposure time, and typical force–distance curves measured in HOCl/PAA and changes in pull-off forces over immersion time for PAA are given; supplementary Tables S1 and S2 contain the characteristic Δf and t values for all experimental replicates, and Tables S3 and S4 list all of the replicates of the kinetic parameters obtained from fitting various models to the HOCl/PAA-exposed polyamide films in sorption/degradation stages (PDF)

■ AUTHOR INFORMATION

Corresponding Authors

Ning Dai – *Department of Civil, Structural and Environmental Engineering, University at Buffalo, Buffalo, New York 14260, United States;* orcid.org/0000-0002-

https://doi.org/10.1021/acs.langmuir.1c02835
Langmuir XXXX, XXX, XXX–XXX

8468-5611; Phone: (716) 645-4015; Email: ningdai@buffalo.edu

Prathima C. Nalam − *Department of Materials Design and Innovation, University at Buffalo, Buffalo, New York 14260, United States;* orcid.org/0000-0002-7355-4931; Phone: (716) 645-9193; Email: prathima@buffalo.edu

Author

Tashfia M. Mohona − *Department of Civil, Structural and Environmental Engineering, University at Buffalo, Buffalo, New York 14260, United States*

Complete contact information is available at: https://pubs.acs.org/10.1021/acs.langmuir.1c02835

Author Contributions

T.M.M. performed all of the experiments described in the manuscript and analyzed the data. N.D. and P.C.N. designed the project and guided T.M.M. in the experimental design and data analysis. The manuscript was written through contributions of all authors. All authors have given approval to the final version of the manuscript.

Funding

This work was supported by the National Science Foundation (CBET-1652412). This work made use of the Cornell Center for Materials Research Shared Facilities, which are supported through the NSF MRSEC program (DMR-1719875). This work was also partially supported by the Mark Diamond Research Fund of the Graduate Student Association at the University at Buffalo, The State University of New York.

Notes

The authors declare no competing financial interest.

■ ACKNOWLEDGMENTS

The authors would like to thank Drs. Haiqing Lin and Mark Swihart from the Department of Chemical and Biological Engineering, UB, for providing access to spin-coater and glovebox, respectively, and Dr. Andrea Arcifa from the EMPA (Swiss Federal Laboratories for Materials Science and Technology), Dübendorf, Switzerland, for useful discussions on their XPS results.

■ REFERENCES

(1) Werber, J. R.; Osuji, C. O.; Elimelech, M. Materials for Next-Generation Desalination and Water Purification Membranes. *Nat. Rev. Mater.* **2016**, *1*, No. 16018.

(2) Antony, A.; Fudianto, R.; Cox, S.; Leslie, G. Assessing the Oxidative Degradation of Polyamide Reverse Osmosis Membrane-Accelerated Ageing with Hypochlorite Exposure. *J. Membr. Sci.* **2010**, *347*, 159−164.

(3) Verbeke, R.; Gómez, V.; Vankelecom, I. F. J. Chlorine-Resistance of Reverse Osmosis (RO) Polyamide Membranes. *Prog. Polym. Sci.* **2017**, *72*, 1−15.

(4) Lau, W. J.; Ismail, A. F.; Misdan, N.; Kassim, M. A. A Recent Progress in Thin Film Composite Membrane: A Review. *Desalination* **2012**, *287*, 190−199.

(5) Brodtmann, N. V., Jr; Russo, P. J. The Use of Chloramine for Reduction of Trihalomethanes and Disinfection of Drinking Water. *J. - Am. Water Works Assoc.* **1979**, *71*, 40−42.

(6) *Filmtec Reverse Osmosis Membrane*, Technical Manual, Form No. 609-007101009; Dow Water & Process Solutions, 2011.

(7) Kang, G. D.; Gao, C. J.; Chen, W. D.; Jie, X. M.; Cao, Y. M.; Yuan, Q. Study on Hypochlorite Degradation of Aromatic Polyamide Reverse Osmosis Membrane. *J. Membr. Sci.* **2007**, *300*, 165−171.

(8) Ling, R.; Shao, J. H.; Chen, J. P.; Reinhard, M. Iron Catalyzed Degradation of an Aromatic Polyamide Reverse Osmosis Membrane by Free Chlorine. *J. Membr. Sci.* **2019**, *577*, 205−211.

(9) Kwon, Y. N.; Leckie, J. O. Hypochlorite Degradation of Crosslinked Polyamide Membranes - II. Changes in Hydrogen Bonding Behavior and Performance. *J. Membr. Sci.* **2006**, *282*, 456−464.

(10) Stolov, M.; Freger, V. Degradation of Polyamide Membranes Exposed to Chlorine: An Impedance Spectroscopy Study. *Environ. Sci. Technol.* **2019**, *53*, 2618−2625.

(11) Orton, K. J. P.; Soper, F. G.; Williams, G. CXXXII.—The Chlorination of Anilides. Part III. N-Chlorination and C-Chlorination as Simultaneous Side Reactions. *J. Chem. Soc.* **1928**, 998−1005.

(12) Kwon, Y. N.; Tang, C. Y.; Leckie, J. O. Change of Membrane Performance Due to Chlorination of Crosslinked Polyamide Membranes. *J. Appl. Polym. Sci.* **2006**, *102*, 5895−5902.

(13) Ling, R.; Yu, L.; Pham, T. P. T.; Shao, J. H.; Chen, J. P.; Reinhard, M. The Tolerance of a Thin-Film Composite Polyamide Reverse Osmosis Membrane to Hydrogen Peroxide Exposure. *J. Membr. Sci.* **2017**, *524*, 529−536.

(14) Yu, L.; Ling, R.; Chen, J. P.; Reinhard, M. Quantitative Assessment of the Iron-Catalyzed Degradation of a Polyamide Nanofiltration Membrane by Hydrogen Peroxide. *J. Membr. Sci.* **2019**, *588*, No. 117154.

(15) Bianchini, R.; Calucci, L.; Lubello, C.; Pinzino, C. Intermediate Free Radicals in the Oxidation of Wastewaters. *Res. Chem. Intermed.* **2002**, *28*, 247−256.

(16) van den Broek, W. B. P.; Boorsma, M. J.; Huiting, H.; Dusamos, M. G.; van Agtmaal, S. Prevention of Biofouling in Industrial RO Systems: Experiences with Peracetic Acid. *Water Pract. Technol.* **2010**, *5*, wpt2010042.

(17) Wagner, M.; Brumelis, D.; Gehr, R. Disinfection of Wastewater by Hydrogen Peroxide or Peracetic Acid: Development of Procedures for Measurement of Residual Disinfectant and Application to a Physicochemically Treated Municipal Effluent. *Water Environ. Res.* **2002**, *74*, 33−50.

(18) Hassaballah, A. H.; Bhatt, T.; Nyitrai, J.; Dai, N.; Sassoubre, L. Inactivation of *E. coli*, Enterococcus Spp., Somatic Coliphage, and Cryptosporidium Parvum in Wastewater by Peracetic Acid (PAA), Sodium Hypochlorite, and Combined PAA-Ultraviolet Disinfection. *Environ. Sci.: Water Res. Technol.* **2020**, *6*, 197−209.

(19) Hassaballah, A. H.; Nyitrai, J.; Hart, C. H.; Dai, N.; Sassoubre, L. M. A Pilot-Scale Study of Peracetic Acid and Ultraviolet Light for Wastewater Disinfection. *Environ. Sci.: Water Res. Technol.* **2019**, *5*, 1453−1463.

(20) Veschetti, E.; Cutilli, D.; Bonadonna, L.; Briancesco, R.; Martini, C.; Cecchini, G.; Anastasi, P.; Ottaviani, M. Pilot-plant Comparative Study Of Peracetic Acid And Sodium Hypochlorite Wastewater Disinfection. *Water Res.* **2003**, *37*, 78−94.

(21) Ghafari, M.; Mohona, T. M.; Su, L.; Lin, H.; Plata, D.; Xiong, B.; Dai, N. Effects of Peracetic Acid on Aromatic Polyamide Nanofiltration Membranes: A Comparative Study with Chlorine. *Environ. Sci.: Water Res. Technol.* **2021**, *7*, 306−320.

(22) Reviakine, I.; Johannsmann, D.; Richter, R. P. Hearing What You Cannot See and Visualizing What You Hear: Interpreting Quartz Crystal Microbalance Data from Solvated Interfaces. *Anal. Chem.* **2011**, *83*, 8838−8848.

(23) Schumacher, R. The Quartz Microbalance: A Novel Approach to the in-situ Investigation of Interfacial Phenomena at the Solid/Liquid Junction. *Angew. Chem., Int. Ed.* **1990**, *29*, 329−343.

(24) Huang, R. X.; Yi, P.; Tang, Y. Z. Probing the Interactions of Organic Molecules, Nanomaterials, and Microbes with Solid Surfaces using Quartz Crystal Microbalances: Methodology, Advantages, and Limitations. *Environ. Sci.: Processes Impacts* **2017**, *19*, 793−811.

(25) Chen, Q.; Xu, S. M.; Liu, Q. X.; Masliyah, J.; Xu, Z. H. QCM-D Study of Nanoparticle Interactions. *Adv. Colloid Interface Sci.* **2016**, *233*, 94−114.

(26) Zhang, G. Z.; Wu, C. Quartz Crystal Microbalance Studies on Conformational Change of Polymer Chains at Interface. *Macromol. Rapid Commun.* **2009**, *30*, 328−335.
(27) Raudino, M.; Giamblanco, N.; Montis, C.; Berti, D.; Marletta, G.; Baglioni, P. Probing the Cleaning of Polymeric Coatings by Nanostructured Fluids: A QCM-D Study. *Langmuir* **2017**, *33*, 5675−5684.
(28) Feiler, A. A.; Sahlholm, A.; Sandberg, T.; Caldwell, K. D. Adsorption and Viscoelastic Properties of Fractionated Mucin (BSM) and Bovine Serum Albumin (BSA) Studied with Quartz Crystal Microbalance (QCM-D). *J. Colloid Interface Sci.* **2007**, *315*, 475−481.
(29) Tammelin, T.; Merta, J.; Johansson, L. S.; Stenius, P. Viscoelastic Properties of Cationic Starch Adsorbed on Quartz Studied by QCM-D. *Langmuir* **2004**, *20*, 10900−10909.
(30) Turon, X.; Rojas, O. J.; Deinhammer, R. S. Enzymatic Kinetics of Cellulose Hydrolysis: A QCM-D Study. *Langmuir* **2008**, *24*, 3880−3887.
(31) Hu, G.; Heitmann, J. A.; Rojas, O. J. In situ Monitoring of Cellulase Activity by Microgravimetry with a Quartz Crystal Microbalance. *J. Phys. Chem. B* **2009**, *113*, 14761−14768.
(32) Yao, J. W.; Xiao, Y.; Zuo, Q. L.; Zhang, Y.; Tao, T.; Lin, C. J. Effectiveness of Cysteine Proteases on Protein/Pigment Film Removal. *Arch. Oral Biol.* **2013**, *58*, 1618−1626.
(33) Yao, J. W.; Lin, C. J.; Tao, T.; Lin, F. The Effect of Various Concentrations of Papain on the Properties and Hydrolytic Rates of Beta-Casein Layers. *Colloids Surf., B* **2013**, *101*, 272−279.
(34) Craig, M.; Bordes, R.; Holmberg, K. Polypeptide Multilayer Self-Assembly and Enzymatic Degradation on Tailored Gold Surfaces Studied by QCM-D. *Soft Matter* **2012**, *8*, 4788−4794.
(35) Hou, Y.; Chen, J.; Sun, P.; Gan, Z.; Zhang, G. In-situ Investigations on Enzymatic Degradation of Poly(ε-Caprolactone). *Polymer* **2007**, *48*, 6348−6353.
(36) Cometa, S.; Bartolozzi, I.; Corti, A.; Chiellini, F.; De Giglio, E.; Chiellini, E. Hydrolytic and Microbial Degradation of Multi-Block Polyurethanes Based on Poly(ε-Caprolactone)/Poly(Ethylene Glycol) Segments. *Polym. Degrad. Stab.* **2010**, *95*, 2013−2021.
(37) Yang, J. X.; Li, L. W.; Ma, C. F.; Ye, X. D. Degradable Polyurethane with Poly(2-Ethyl-2-Oxazoline) Brushes for Protein Resistance. *RSC Adv.* **2016**, *6*, 69930−69938.
(38) Clegg, J. R.; Ludolph, C. M.; Peppas, N. A. QCM-D Assay for Quantifying the Swelling, Biodegradation, and Protein Adsorption of Intelligent Nanogels. *J. Appl. Polym. Sci.* **2020**, *137*, 48655.
(39) Ying, W.; Siebdrath, N.; Uhl, W.; Gitis, V.; Herzberg, M. New Insights on Early Stages of RO Membranes Fouling During Tertiary Wastewater Desalination. *J. Membr. Sci.* **2014**, *466*, 26−35.
(40) Tirado, M. L. M.; Bass, M.; Piatkovsky, M.; Ulbricht, M.; Herzberg, M.; Freger, V. Assessing Biofouling Resistance of a Polyamide Reverse Osmosis Membrane Surface-Modified with a Zwitterionic Polymer. *J. Membr. Sci.* **2016**, *520*, 490−498.
(41) Ferrando, D.; Toubiana, D.; Kandiyote, N. S.; Nguyen, T. H.; Nejidat, A.; Herzberg, M. Ambivalent Role of Calcium in the Viscoelastic Properties of Extracellular Polymeric Substances and the Consequent Fouling of Reverse Osmosis Membranes. *Desalination* **2018**, *429*, 12−19.
(42) Ishigami, T.; Amano, K.; Fujii, A.; Ohmukai, Y.; Kamio, E.; Maruyama, T.; Matsuyama, H. Fouling Reduction of Reverse Osmosis Membrane by Surface Modification via Layer-By-Layer Assembly. *Sep. Purif. Technol.* **2012**, *99*, 1−7.
(43) Sweity, A.; Oren, Y.; Ronen, Z.; Herzberg, M. The Influence of Antiscalants on Biofouling of RO Membranes in Seawater Desalination. *Water Res.* **2013**, *47*, 3389−3398.
(44) Wu, J. J.; Contreras, A. E.; Li, Q. L. Studying the Impact of RO Membrane Surface Functional Groups on Alginate Fouling in Seawater Desalination. *J. Membr. Sci.* **2014**, *458*, 120−127.
(45) Zhang, S.; Ly, Q. V.; Nghiem, L. D.; Wang, J.; Li, J.; Hu, Y. Optimization and Organic Fouling Behavior of Zwitterion-Modified Thin-Film Composite Polyamide Membrane for Water Reclamation: A Comprehensive Study. *J. Membr. Sci.* **2020**, *596*, 117748.
(46) Lin, N. H.; Cohen, Y. QCM Study of Mineral Surface Crystallization on Aromatic Polyamide Membrane Surfaces. *J. Membr. Sci.* **2011**, *379*, 426−433.
(47) Shaffer, D. L.; Tousley, M. E.; Elimelech, M. Influence of Polyamide Membrane Surface Chemistry on Gypsum Scaling Behavior. *J. Membr. Sci.* **2017**, *525*, 249−256.
(48) Kearney, L. T.; Howarter, J. A. QCM-based Measurement of Chlorine-Induced Polymer Degradation Kinetics. *Langmuir* **2014**, *30*, 8923−8930.
(49) Powell, J.; Luh, J.; Coronell, O. Bulk Chlorine Uptake by Polyamide Active Layers of Thin-Film Composite Membranes Upon Exposure to Free Chlorine-Kinetics, Mechanisms, and Modeling. *Environ. Sci. Technol.* **2014**, *48*, 2741−2749.
(50) Powell, J.; Luh, J.; Coronell, O. Amide Link Scission in the Polyamide Active Layers of Thin-Film Composite Membranes Upon Exposure to Free Chlorine: Kinetics and Mechanisms. *Environ. Sci. Technol.* **2015**, *49*, 12136−12144.
(51) Do, V. T.; Tang, C. Y. Y.; Reinhard, M.; Leckie, J. O. Effects of Chlorine Exposure Conditions on Physiochemical Properties and Performance of a Polyamide Membrane- Mechanisms and Implications. *Environ. Sci. Technol.* **2012**, *46*, 13184−13192.
(52) Chan, E. P.; Lee, J. H.; Chung, J. Y.; Stafford, C. M. An Automated Spin-Assisted Approach for Molecular Layer-By-Layer Assembly of Crosslinked Polymer Thin Films. *Rev. Sci. Instrum.* **2012**, *83*, 114102.
(53) Johnson, P. M.; Yoon, J.; Kelly, J. Y.; Howarter, J. A.; Stafford, C. M. Molecular Layer-By-Layer Deposition of Highly Crosslinked Polyamide Films. *J. Polym. Sci., Part B: Polym. Phys.* **2012**, *50*, 168−173.
(54) Shaffer, D. L.; Feldman, K. E.; Chan, E. P.; Stafford, G. R.; Stafford, C. M. Characterizing Salt Permeability in Polyamide Desalination Membranes Using Electrochemical Impedance Spectroscopy. *J. Membr. Sci.* **2019**, *583*, 248−257.
(55) Tousley, M. E.; Shaffer, D. L.; Lee, J. H.; Osuji, C. O.; Elimelech, M. Effect of Final Monomer Deposition Steps on Molecular Layer-By-Layer Polyamide Surface Properties. *Langmuir* **2016**, *32*, 10815−10823.
(56) Gu, J. E.; Lee, S.; Stafford, C. M.; Lee, J. S.; Choi, W.; Kim, B. Y.; Baek, K. Y.; Chan, E. P.; Chung, J. Y.; Bang, J.; Lee, J. H. Molecular Layer-By-Layer Assembled Thin-Film Composite Membranes for Water Desalination. *Adv. Mater.* **2013**, *25*, 4778−4782.
(57) Wang, J. B.; Kingsbury, R. S.; Perry, L. A.; Coronell, O. Partitioning of Alkali Metal Salts and Boric Acid from Aqueous Phase into the Polyamide Active Layers of Reverse Osmosis Membranes. *Environ. Sci. Technol.* **2017**, *51*, 2295−2303.
(58) Lin, L.; Lopez, R.; Ramon, G. Z.; Coronell, O. Investigating the Void Structure of the Polyamide Active Layers of Thin-Film Composite Membranes. *J. Membr. Sci.* **2016**, *497*, 365−376.
(59) Perry, L. A.; Coronell, O. Reliable, Bench-Top Measurements of Charge Density in the Active Layers of Thin-Film Composite and Nanocomposite Membranes Using Quartz Crystal Microbalance Technology. *J. Membr. Sci.* **2013**, *429*, 23−33.
(60) Ying, W.; Gitis, V.; Lee, J.; Herzberg, M. Effects of Shear Rate on Biofouling of Reverse Osmosis Membrane During Tertiary Wastewater Desalination. *J. Membr. Sci.* **2013**, *427*, 390−398.
(61) Vig, J. R. UV/Ozone Cleaning of Surfaces. *J. Vac. Sci. Technol., A* **1985**, *3*, 1027−1034.
(62) Zhang, M. X.; Wiener, C. G.; Sepulveda-Medina, P. I.; Douglas, J. F.; Vogt, B. D. Influence of Sodium Salts on the Swelling and Rheology of Hydrophobically Cross-Linked Hydrogels Determined by QCM-D. *Langmuir* **2019**, *35*, 16612−16623.
(63) Coronell, O.; Marinas, B. J.; Zhang, X. J.; Cahill, D. G. Quantification of Functional Groups and Modeling of their Ionization Behavior in the Active Layer of FT30 Reverse Osmosis Membrane. *Environ. Sci. Technol.* **2008**, *42*, 5260−5266.
(64) Morris, J. C. The Acid Ionization Constant of HOCl from 5 to 35°. *J. Phys. Chem. A* **1966**, *70*, 3798−3805.
(65) National Center for Biotechnology Information. PubChem Compound Summary for CID 6585, Peracetic acid.

https://doi.org/10.1021/acs.langmuir.1c02835
Langmuir XXXX, XXX, XXX−XXX

(66) Freger, V. Swelling and Morphology of the Skin Layer of Polyamide Composite Membranes: An Atomic Force Microscopy Study. *Environ. Sci. Technol.* **2004**, *38*, 3168−3175.
(67) Escoda, A.; Fievet, P.; Lakard, S.; Szymczyk, A.; Deon, S. Influence of Salts on the Rejection of Polyethyleneglycol by an NF Organic Membrane: Pore Swelling and Salting-Out Effects. *J. Membr. Sci.* **2010**, *347*, 174−182.
(68) Hutter, J. L.; Bechhoefer, J. Calibration of Atomic Force Microscope Tips. *Rev. Sci. Instrum.* **1993**, *64*, 1868−1873.
(69) Akin, O.; Temelli, F. Probing the Hydrophobicity of Commercial Reverse Osmosis Membranes Produced by Interfacial Polymerization Using Contact Angle, XPS, FTIR, FE-SEM and AFM. *Desalination* **2011**, *278*, 387−396.
(70) Khorshidi, B.; Thundat, T.; Fleck, B. A.; Sadrzadeh, M. Thin Film Composite Polyamide Membranes: Parametric Study on the Influence of Synthesis Conditions. *RSC Adv.* **2015**, *5*, 54985−54997.
(71) Khorshidi, B.; Thundat, T.; Fleck, B. A.; Sadrzadeh, M. A Novel Approach Toward Fabrication of High Performance Thin Film Composite Polyamide Membranes. *Sci. Rep.* **2016**, *6*, 22069.
(72) Sauerbrey, G. Verwendung von Schwingquarzen zur Wägung dünner Schichten und zur Mikrowägung. *Z. Phys.* **1959**, *155*, 206−222.
(73) Reed, L. J.; Berkson, J. The Application of the Logistic Function to Experimental Data. *J. Phys. Chem. B* **1929**, *33*, 760−779.
(74) Navarro-Verdugo, A. L.; Goycoolea, F. M.; Romero-Melendez, G.; Higuera-Ciapara, I.; Arguelles-Monal, W. A Modified Boltzmann Sigmoidal Model for the Phase Transition of Smart Gels. *Soft Matter* **2011**, *7*, 5847−5853.
(75) Yongabi, D.; Khorshid, M.; Gennaro, A.; Jooken, S.; Duwe, S.; Deschaume, O.; Losada-Perez, P.; Dedecker, P.; Bartic, C.; Wubbenhorst, M.; Wagner, P. QCM-D Study of Time-Resolved Cell Adhesion and Detachment: Effect of Surface Free Energy on Eukaryotes and Prokaryotes. *ACS Appl. Mater. Interfaces* **2020**, *12*, 18258−18272.
(76) Fang, D.; Zhuang, X.; Huang, L.; Zhang, Q.; Shen, Q.; Jiang, L.; Xu, X.; Ji, F. Developing the New Kinetics Model Based on the Adsorption Process: From Fitting to Comparison and Prediction. *Sci. Total Environ.* **2020**, *725*, 138490.
(77) Wang, J.; Guo, X. Adsorption Kinetic Models: Physical Meanings, Applications, and Solving Methods. *J. Hazard. Mater.* **2020**, *390*, 122156.
(78) Sedeva, I. G.; Fornasiero, D.; Ralston, J.; Beattie, D. A. The Influence of Surface Hydrophobicity on Polyacrylamide Adsorption. *Langmuir* **2009**, *25*, 4514−4521.
(79) Lagergren, S. K. About the Theory of So-Called Adsorption of Soluble Substances. *K. Sven. Vetensk.-Akad. Handl.* **1898**, *24*, 1−39.
(80) Li, Q.; Yue, Q. Y.; Su, Y.; Gao, B. Y.; Li, J. Two-Step Kinetic Study on the Adsorption and Desorption of Reactive Dyes at Cationic Polymer/Bentonite. *J. Hazard. Mater.* **2009**, *165*, 1170−1178.
(81) Tang, C. Y. Y.; Kwon, Y. N.; Leckie, J. O. Probing the Nano- And Micro-Scales of Reverse Osmosis Membranes—A Comprehensive Characterization of Physiochemical Properties of Uncoated and Coated Membranes by XPS, TEM, ATR-FTIR, and Streaming Potential Measurements. *J. Membr. Sci.* **2007**, *287*, 146−156.
(82) Mondal, S.; Wickramasinghe, S. R. Produced Water Treatment by Nanofiltration and Reverse Osmosis Membranes. *J. Membr. Sci.* **2008**, *322*, 162−170.
(83) Kwak, S. Y.; Jung, S. G.; Kim, S. H. Structure-Motion-Performance Relationship of Flux-Enhanced Reverse Osmosis (RO) Membranes Composed of Aromatic Polyamide Thin Films. *Environ. Sci. Technol.* **2001**, *35*, 4334−4340.
(84) Nalam, P. C.; Daikhin, L.; Espinosa-Marzal, R. M.; Clasohm, J.; Urbakh, M.; Spencer, N. D. Two-Fluid Model for the Interpretation of Quartz Crystal Microbalance Response: Tuning Properties of Polymer Brushes with Solvent Mixtures. *J. Phys. Chem. C* **2013**, *117*, 4533−4543.
(85) Shoaib, T.; Nalam, P. C.; He, Y. C.; Chen, Y. T.; Espinosa-Marzal, R. M. Assembly, Morphology, Diffusivity, and Indentation of Hydrogel-Supported Lipid Bilayers. *Langmuir* **2017**, *33*, 7105−7117.
(86) Xu, J.; Wang, Z.; Wei, X. Y.; Yang, S. B.; Wang, J. X.; Wang, S. C. The Chlorination Process of Crosslinked Aromatic Polyamide Reverse Osmosis Membrane: New Insights from the Study of Self-Made Membrane. *Desalination* **2013**, *313*, 145−155.
(87) Kawaguchi, T.; Tamura, H. Chlorine-Resistant Membrane for Reverse Osmosis. I. Correlation Between Chemical Structures and Chlorine Resistance of Polyamides. *J. Appl. Polym. Sci.* **1984**, *29*, 3359−3367.
(88) Beamson, G.; Briggs, D. High Resolution XPS of Organic Polymers: The Scienta ESCA300 Database. *J. Chem. Educ.* **1993**, *70*, A25.
(89) Laroche, G.; Fitremann, J.; Gherardi, N. FTIR-ATR Spectroscopy in Thin Film Studies: The Importance of Sampling Depth and Deposition Substrate. *Appl. Surf. Sci.* **2013**, *273*, 632−637.
(90) Kang, E.; Ti, H.; Neoh, K. XPS Studies of Some Chemically Synthesized Polypyrrole−Organic Acceptor Complexes. *Polym. J.* **1988**, *20*, 845−850.
(91) Ohta, T.; Yamada, M.; Kuroda, H. X-ray Photoelectron Spectroscopy of p-Benzoquinone, Hydroquinone and Their Halogen-Substituted Derivatives. *Bull. Chem. Soc. Jpn.* **1974**, *47*, 1158−1161.
(92) Zhu, J.; Pan, J. S.; Ma, C. F.; Zhang, G. Z.; Liu, G. M. Specific Ion Effects on the Enzymatic Degradation of Polymeric Marine Antibiofouling Materials. *Langmuir* **2019**, *35*, 11157−11166.
(93) Urbakh, M.; Daikhin, L. Roughness Effect on the Frequency of a Quartz-Crystal Resonator in Contact with a Liquid. *Phys. Rev. B* **1994**, *49*, 4866−4870.
(94) Wang, T.; Wang, X. W.; Long, Y. C.; Liu, G. M.; Zhang, G. Z. Ion-Specific Conformational Behavior of Polyzwitterionic Brushes: Exploiting it for Protein Adsorption/Desorption Control. *Langmuir* **2013**, *29*, 6588−6596.
(95) Gutig, C.; Grady, B. P.; Striolo, A. Experimental Studies on the Adsorption of Two Surfactants on Solid-Aqueous Interfaces: Adsorption Isotherms and Kinetics. *Langmuir* **2008**, *24*, 4806−4816.
(96) Thavorn, J.; Hamon, J. J.; Kitiyanan, B.; Striolo, A.; Grady, B. P. Competitive Surfactant Adsorption of AOT and TWEEN 20 on Gold Measured Using a Quartz Crystal Microbalance with Dissipation. *Langmuir* **2014**, *30*, 11031−11039.
(97) Rodahl, M.; Hook, F.; Krozer, A.; Brzezinski, P.; Kasemo, B. Quartz-Crystal Microbalance Setup for Frequency and Q-Factor Measurements in Gaseous and Liquid Environments. *Rev. Sci. Instrum.* **1995**, *66*, 3924−3930.
(98) Vogt, B. D.; Lin, E. K.; Wu, W. L.; White, C. C. Effect of Film Thickness on the Validity of the Sauerbrey Equation for Hydrated Polyelectrolyte Films. *J. Phys. Chem. B* **2004**, *108*, 12685−12690.
(99) Románszki, L.; Tatarko, M.; Jiao, M.; Keresztes, Z.; Hianik, T.; Thompson, M. Casein Probe−based Fast Plasmin Determination in the Picomolar Range by an Ultra-High Frequency Acoustic Wave Biosensor. *Sens. Actuators, B* **2018**, *275*, 206−214.
(100) Goda, T.; Miyahara, Y. Interpretation of Protein Adsorption Through its Intrinsic Electric Charges: A Comparative Study Using a Field-Effect Transistor, Surface Plasmon Resonance, and Quartz Crystal Microbalance. *Langmuir* **2012**, *28*, 14730−14738.
(101) Iler, R. K. *The Chemistry of Silica*, 1st ed.; John Wiley & Sons: New York, 1979; pp 97−99.
(102) Coronell, O.; Marinas, B. J.; Cahill, D. G. Depth Heterogeneity of Fully Aromatic Polyamide Active Layers in Reverse Osmosis and Nanofiltration Membranes. *Environ. Sci. Technol.* **2011**, *45*, 4513−4520.

https://doi.org/10.1021/acs.langmuir.1c02835
Langmuir XXXX, XXX, XXX−XXX